Extrinsic Localized Excitons in Patterned 2D Semiconductors

Denis Yagodkin, Kyrylo Greben, Alberto Eljarrat, Sviatoslav Kovalchuk, Mahdi Ghorbani-Asl, Mitisha Jain, Silvan Kretschmer, Nikolai Severin, Jürgen P. Rabe, Arkady V. Krasheninnikov, Christoph T. Koch, and Kirill I. Bolotin*

A new localized excitonic state is demonstrated in patterned monolayer 2D semiconductors. The signature of an exciton associated with that state is observed in the photoluminescence spectrum after electron beam exposure of several 2D semiconductors. The localized state, which is distinguished by non-linear power dependence, survives up to room temperature and is patternable down to 20 nm resolution. The response of the new exciton to the changes of electron beam energy, nanomechanical cleaning, and encapsulation via multiple microscopic, spectroscopic, and computational techniques is probed. All these approaches suggest that the state does not originate from irradiation-induced structural defects or spatially non-uniform strain, as commonly assumed. Instead, it is shown to be of extrinsic origin, likely a charge transfer exciton associated with the organic substance deposited onto the 2D semiconductor. By demonstrating that structural defects are not required for the formation of localized excitons, this work opens new possibilities for further understanding of localized excitons as well as their use in applications that are sensitive to the presence of defects, e.g. chemical sensing and quantum technologies.

D. Yagodkin, K. Greben, S. Kovalchuk, K. I. Bolotin
Department of Physics
Freie Universität Berlin
14195 Berlin, Germany
E-mail: bolotin@zedat.fu-berlin.de
A. Eljarrat, N. Severin, J. P. Rabe, C. T. Koch
Department of Physics & IRIS Adlershof
Humboldt-Universität zu Berlin
12489 Berlin, Germany
M. Ghorbani-Asl, M. Jain, S. Kretschmer, A. V. Krasheninnikov
Helmholtz-Zentrum Dresden-Rossendorf
Institute of Ion Beam Physics and Materials Research
01328 Dresden, Germany
A. V. Krasheninnikov
Department of Applied Physics
Aalto University
02150 Aalto, Finland

1. Introduction

Excitonic complexes in transition metal dichalcogenides (TMDs) are Coulomb-bound states of electrons and holes, which can be broadly classified as either free or localized. Free excitons move about the crystal transmitting information and energy.[1] The properties of these quasiparticles (e.g., neutral and charged, dark and bright free excitons), including their binding energies, formation mechanisms, and valley dynamics have largely been understood both theoretically and experimentally within the last decade.[2,3] In contrast, localized excitons are spatially confined by a sufficiently strong potential. Unlike their free counterparts, localized excitons do not transfer information or energy, couple to both valleys of the TMD, and have a nearly flat energy dispersion.[4–6] Although these states were previously largely ignored, many recent developments suggest that they may determine critical properties of TMDs, such as the diffusion length, the doping response, and the lifetimes of various excitonic species.[1,7] Some types of localized excitons feature charge and spin lifetimes up to microseconds owing to the decoupling from the host crystal.[8,9] These states may play a determining role in the relaxation of excitons in TMD heterostructures by providing pathways for excitations to tunnel between two angle-mismatched TMDs.[7,10] Some localized states behave as single quantum emitters, driving the interest in potential applications in quantum technologies.[6,9,11,12] More recently, single quantum emitters based on localized states in TMDs came under intense scrutiny. These emitters allow precise patterning of the emitting centers, robust control of the emission properties via electrostatic gating, and easy integration with other 2D materials for further photonic processing.[13–15] Nevertheless, the emission from these states has been found to decay with temperature and completely disappear at room temperature. Finally, long-lived localized states induced at the surface of TMDs may potentially be used as sensors of a TMD's environment.[16,17]

While many different types of localized excitons have been observed in different TMDs,[7] the mechanisms leading to their formation as well as their intrinsic properties remain largely unknown. These states are near-universally attributed

to structural disorder in the TMD lattice.[18] The prevalent source of such disorder is lattice vacancies that can be either native[4] or induced using high-energy particles.[19,20] Only very recently, combined local probe spectroscopy studies of ultra-clean encapsulated samples managed to associate a certain localized state with a structural vacancy defect in TMDs.[4,21] Another type of structural disorder appears when a spatially non-uniform strain locally distorts a TMD lattice.[22] Such a strain can lead to the formation of a localized state by creating a spatially varying potential confining the excitons. The nature of such a localized state and the role of structural vacancies in its formation remain debated.[23] Finally, the periodic disorder arising in angle-matched TMD heterostructures (moiré lattices) produces periodic potential wells deep enough to localize excitons.[24–26]

Contrary to the examples discussed above, we demonstrate a controlled and patternable localized state in TMDs that is not related to the intrinsic disorder. We induce a localized excitonic state in a broad family of TMD materials via electron beam irradiation. Multiple key characteristics of this state—its change with the energy of the electrons, the response to nanomechanical cleaning, and the response to hBN encapsulation are not compatible with the structural disorder, such as lattice defects or localized strain. We suggest that the only mechanism that can explain such a state is the formation of a charge-transfer exciton between an organic molecule on the TMD surface and the TMD itself. Our work may potentially clarify the nature of some previously observed localized states and provide avenues to patterning and tuning such states in the future.

2. Results and Discussion

To fabricate a device containing localized states, a monolayer TMD flake is mechanically exfoliated and transferred onto a SiO_2 or hBN substrate (Methods), loaded into an electron microscope where electron beam lithography (EBL) is used to raster an electron beam across the TMD surface. Unless stated otherwise, the acceleration voltage of the electron beam is 10 keV and the dose (fluence of electrons) is varied in the range of 0.5–14 mC cm^{-2} (Note S1, Supporting Information). We raster the beam in a pattern consisting of stripes with a spacing of 80 nm (**Figure 1**a, Methods). This pattern is visible in the atomic force microscopy (AFM) topography images (Figure 1b) of the TMD's surface after exposure without any additional treatment. The exposed regions are ≈0.3 nm higher (bottom panel in Figure 1b) than the unexposed regions. The height profile has a period of ≈80 nm, consistent with the designed e-beam pattern. A similar pattern is also observed using scanning transmission electron microscopy (STEM) of suspended bilayer MoS_2 exposed to a higher electron dose of 14 mC cm^{-2} (Figure 1c) where bilayer was used for better mechanical stability. A single stripe has a width of ≈20 nm and the period between stripes is ≈80 nm (bottom panel in Figure 1c). The appearance of an extra layer of material after exposure to e-beam is known and signals e-beam assisted deposition of molecules onto the surface of MoS_2.[29–31]

In the electron-exposed region of all studied TMD materials, we observe a new peak in the PL spectrum (Figure 1d–f). The feature is seen even at room temperature under ambient conditions (blue curves). It is absent in unexposed areas of the same
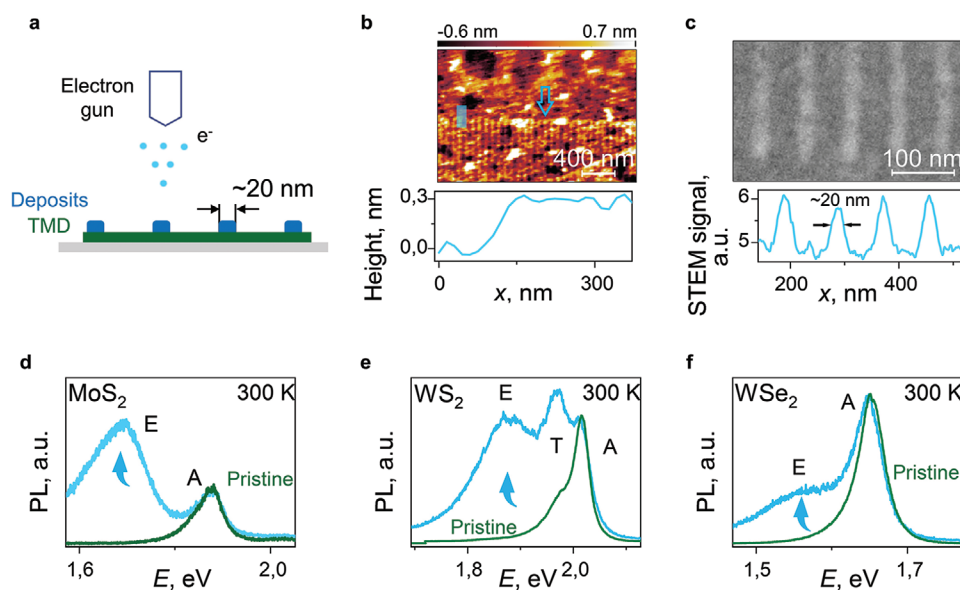

Figure 1. EBL Nanopatterning. a) Local e-beam exposure of TMDs to generate a new excitonic state. b) AFM topography of a 1L-MoS_2 on hBN sample (D1) after e-beam patterning. The period of the lines seen in the image, 80 nm, matches the EBL pattern (vertical lines, cyan arrow). The height profile along the blue line in the image is shown in the bottom panel. c) STEM image of a suspended MoS_2 sample (D2) after EBL along with a line profile (bottom panel). The deposits in the e-beam treated regions of the suspended bilayer MoS_2 are also visible. The width of the stripes, ≈20 nm (bottom panel), and their period, 80 nm, match the parameters of EBL patterning. d–f) Normalized PL spectra from pristine (green curve) and exposed to e-beam (blue curve) areas of MoS_2, WS_2, and WSe_2 correspondingly.
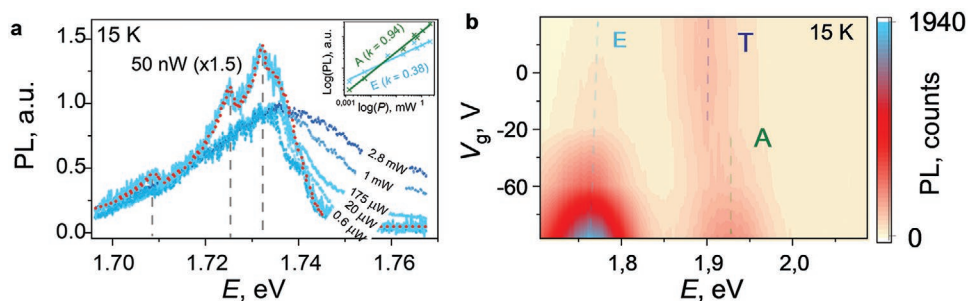
2203060 (2 of 8)

Figure 2. E-beam-related photoluminescence peak and its fluence- and gate-dependencies. a) Normalized PL spectra of e-beam exposed and subsequently hBN encapsulated 1L-MoS$_2$ (sample D3) at 15 K, measured at excitation powers ranging from 50 nW (solid blue curve, multiplied by x1.5 for better visibility) to 2.8 mW. Inset: Power dependence of the area under the E-peak (blue) and A-peak in PL (green). The E-peak has a sublinear dependence on power (linear fit to the data has a slope of 0.4) which is expected for a localized state. b) Low-temperature PL spectra of the modified MoS$_2$ flake on SiO$_2$/Si substrate (sample D4) at back gate voltages from −80 to 20 V.

device before patterning (green curves), as well as in other pristine TMD samples or on e-beam treated bare substrates. The peak is well-separated from native neutral ("A") and charged ("T") excitons in TMDs.[32,33] We tentatively label this new feature "E peak" and turn to the investigation of its properties and origin. Given the similar behavior of all TMD materials, in further discussion, we focus on MoS$_2$ as the most studied member of the group with well-characterized localized states.[4,18,27,28]

We start by studying the low-temperature PL spectra of the patterned MoS$_2$ device. **Figure 2**a shows PL spectra of the sample at 15 K under an excitation power of 50 nW – 2.8 mW (Methods). The spectrum at high fluence consists of a 40 meV wide E peak centered at 1.735 eV and a shoulder of another peak at 1.77 eV (Figure S1, Supporting Information). The 1.77 eV peak is commonly attributed to native defect-bound excitons in MoS$_2$.[18,27,28] At lower fluence, emission of all other excitons is suppressed (Figures 2 and S2, Supporting Information) while sharp features within the E peak emerge (vertical dashed lines). The FWHM of these features of ≈1 meV is much smaller compared to the FWHM of free excitons, 8 meV (Figure S1, Supporting Information). The intensity of the E peak exhibits a sub-linear power dependence ($I\sim P^{0.4}$), compared to the linear dependence of free excitons (Figure 2a, inset and S2, Supporting Information). This is a tell-tale sign of a localized state as its density is limited by the concentration of localized sites.[4,34,35] The overall spectral shape is likely a combination of multiple narrow peaks from individual states distributed between 1.70 and 1.74 eV due to the varying dielectric background.[17,36] Localized emitters with similar power dependence have been observed in various 2D materials and attributed to structural disorder.[4,7,35,37,38] Notably, while previously reported defect-related excitonic peaks in TMDs are only observed at cryogenic temperature,[18–20,27,28] the E peak persists up to room temperature (Figure 1d–f).

Next, we study the dependence of the state on the density of free carriers. We apply a gate voltage, V_g, between the Si backgate and the 1L-MoS$_2$. We observe that the E peak intensity is strongly V_g-dependent with the maximum observed at negative V_g (Figure 2b). The E peak is absent in the pristine region at any voltage (Figure S3, Supporting Information). By examining the intensities of neutral (A) and negatively-charged (T) excitonic peaks at 1.93 and 1.90 eV respectively, we estimate the

Fermi level position, as the increase of T and the decrease of A peaks indicate the filling of the conduction band.[18] The E peak is visible in the range of gate voltages corresponding to the Fermi level being close to the bottom of the conduction band of MoS$_2$. Such a gate voltage dependence has also been observed for other types of localized excitons.[4] It suggests that the E peak involves a shallow donor state inside the bandgap of MoS$_2$ close to the conduction band which is filled at positive gate voltage.[18] The donor nature of the state is further supported by a slight increase of the negatively-charged exciton intensity after e-beam treatment (that is better seen in Figure 1e). The occupancy of that defect state changes with gate voltage producing the observed variation in the associated exciton emission.[14,39] The electrical tunability of this state provides a simple tool for its control.[15]

Having established that the E peak seen in Figures 1 and 2 is caused by a localized state, we now investigate its origin. The most straightforward explanation would be that the state is related to the structural defect produced by e-beam exposure.[40–42] To test this hypothesis, we vary the electron energy from 1.6 to 30 keV while keeping the dose constant and examine the resulting changes in the PL spectra. We interpret the ratio between the integrated areas under the E- and A-peak as proportional to the density of localized excitons (Figure S4, Supporting Information). We observe a fivefold increase in the inferred density of localized excitons for the same dose in the energy range 1.6–4.5 keV (points in **Figure 3**a). The peak ratio (and hence the density of localized excitons) remains non-zero down to low electron energies (<5 keV) and decreases with energies above 10 keV.

The electron energy dependence of the inferred density of localized excitons is different compared to what is expected from structural defects induced by electron irradiation in 2D TMDs. In general, the formation of such defects by a combination of electronic excitations and knock-on damage requires electrons with an energy of at least 30 keV, and the density of structural defects should increase with the electron energy in the entire energy range.[42,43] The presence of a sharp peak in Figure 3a contradicts this scenario. These defects can also appear at lower (≈100 eV) energies due to chemical etching resulting from radicals produced by the beam through electronic excitations,[44] but this mechanism is negligible for the electron energy range used here.
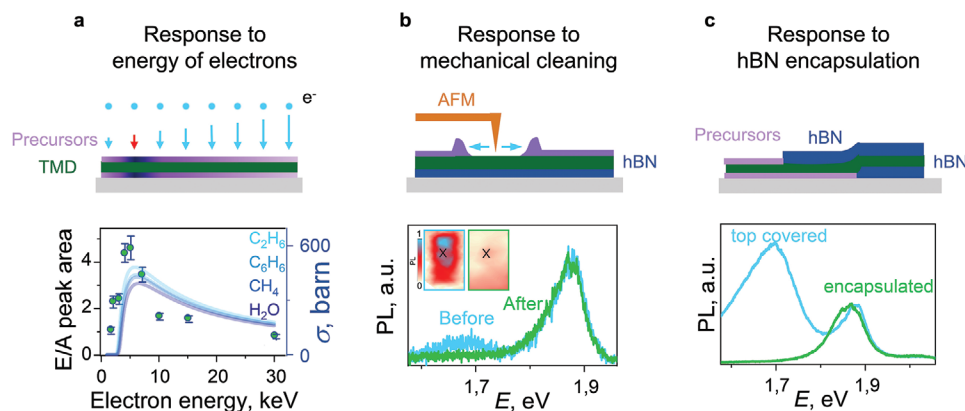
**ADVANCED
SCIENCE NEWS**
www.advancedsciencenews.com

**ADVANCED
FUNCTIONAL
MATERIALS**
www.afm-journal.de

Figure 3. Probing the origin of localized states. a) Ratio of the areas under the E- and A-peak in PL in the exposed area of the MoS$_2$ sample versus electron beam energy (green dots, left axis). This ratio is proportional to the density of induced localized states. The electron dose was kept constant. Calculated cross-section of electron scissoring of hydrogen in C$_2$H$_6$; C$_6$H$_6$; CH$_4$; H$_2$O through the ballistic displacement of hydrogen atoms (shades of blue, right axis). b) PL spectra of a low-dose e-beam treated region of MoS$_2$ on hBN normalized to A exciton (sample D6) before and after mechanical cleaning with AFM (blue and green curves correspondingly). Inset: spatial maps of integrated E-peak at room temperature before (left) and after (right) AFM cleaning. The PL spectra are taken at the same point marked "X" before and after nanomechanical cleaning. The E-peak completely disappears after that procedure. c) PL spectra of the e-beam treated region of MoS$_2$ (sample D7) covered with hBN (light blue), and fully encapsulated (green). The spectra are normalized to A exciton height. The E peak appears in either top- or bottom hBN (Figure. 3c,b) covered samples, but not in fully encapsulated devices.

The hypothesis that the E-peak is unrelated to TMD structural defects is further supported by two additional experiments. In the first experiment, the MoS$_2$ flake on hBN (for mechanical support) is exposed to a low electron dose (0.14 mC cm^{-2}) in a rectangular area (inset in Figure 3b) and the PL spectrum was recorded (Figure 3b, blue curve). Then, we nanomechanically clean the surface of the TMD using repeated scanning with an AFM tip (the "nano-squeegee" technique[45]) and examine the resulting changes in the PL spectra. To achieve this, we imaged the entire device in an AFM while gradually increasing the contact force up to 35 nN over 12 h. As expected,[45] this procedure squeezed the deposits produced by the e-beam out of the AFM imaging window (Figure S5, Supporting Information). Note that the e-beam dose used in this sample was small, as we found that nanomechanical cleaning is incapable of removing the residues for significantly higher doses. After the procedure, the E peak in the imaged region disappears completely (Figure 3b, green curve). This would not be expected if structural defects were the origin of the E peak. In the second experiment, we used a sample that contains area of MoS$_2$ on SiO$_2$ covered with hBN only on top as well as a MoS$_2$ flake area encapsulated in hBN. After electron exposure, the MoS$_2$ on SiO$_2$ shows a high intensity of the E-peak suggesting that electrons penetrate the thin (8 nm) hBN layer (Figure 3c). In contrast, the E peak does not arise in the region of the same flake encapsulated in hBN. Again, this behavior is not consistent with structural defects whose density should not depend on the presence of a thin bottom hBN layer. We note that this behavior is not due hBN-related changes in optical properties or dielectric screening (Figure S1, Supporting Information).[2,17]

The arguments above prove that the E-peak is not related to lattice defects in the TMD. Other mechanisms commonly invoked to explain the appearance of localized states such as strain-, crystalline phase-, or dielectric- related localization can also be excluded in our case. First, the E-peak-related state does not result from the localization of a neutral exciton due to the varying dielectric environment of MoS$_2$. The observed energy separation between the neutral exciton and the E peak of 195 meV (Figures S1, Supporting Information and 2a) is much larger than the maximum energy shift that can be induced by changes in the dielectric environment, 50 meV.[17,46] Second, the state cannot be explained by the localization of excitons in a spatially inhomogeneous strain field. While such strain can, in principle, localize the excitons,[18,25,39,47–49] the maximum strain estimated from AFM topography is an order of magnitude smaller than what is required for this mechanism to explain our data.[50] Third, local patterning can result in a structural phase transition (2H → 1T) breaking the material into individual quantum dots,[51,52] thereby localizing the excitons. Our STEM imaging (Figure S6, Supporting Information) confirms the uniformity of the crystal lattice across pristine and e-beam exposed regions, contradicting such an argument.

We believe that the only plausible microscopic mechanism behind the localized state consistent with our data is that it relates to organic molecules on the surface of MoS$_2$. Electron beam irradiation is known to both break and modifies organic residues already present on the sample surface.[29–31] Such deposits are observed both in our AFM and STEM images (Figure 1a,b). The disappearance of the E-peak after nanomechanical cleaning (Figure 3b) is consistent with these molecules being squeezed out from the scanning area. The absence of the E-peak in the encapsulated device (Figure 3c) is also consistent with the pristine molecule-free nature of the hBN/TMD/hBN devices.

What is the chemical nature of the organic molecules on the surface of the TMD and how do these molecules influence the E peak formation? We hypothesize that the electron beam radicalizes molecular residues present on the surface by ballistic displacement of H atoms (based on the low energy ≈4.5 keV of the peak in Figure 3a). We used density functional theory
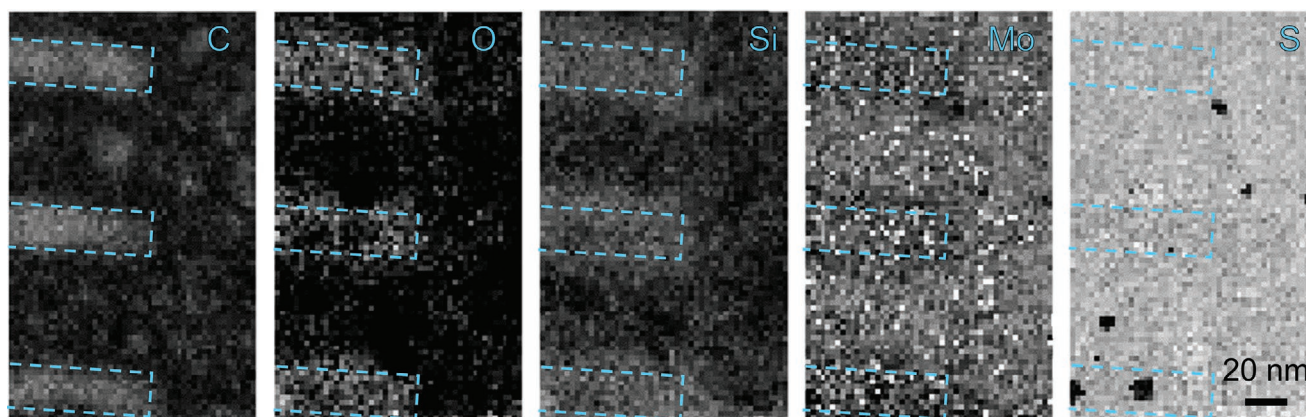
ADVANCED
SCIENCE NEWS
www.advancedsciencenews.com

ADVANCED
FUNCTIONAL
MATERIALS
www.afm-journal.de

Figure 4. Spatial maps of EELS signal for C, O, Si, Mo, and S (white – more intense) across the e-beam patterned region, sample D2 (blue dashed line shows region boundaries). While the EELS signal for Mo and S is uniform across the entire specimen, it surges in the patterned regions for C, O, and Si. Thus, we attributed deposits to organics.

(DFT)-based molecular dynamics to calculate the displacement threshold, T_d (the minimum kinetic energy needed to permanently displace an H atom). We evaluated the displacement thresholds for a range of organic molecules (C_2H_6, C_6H_6, CH_4, and H_2O) for the constrained and free (in parentheses) molecules: $T_d(C_2H_6) = 6.6$ (6.8) eV, $T_d(C_6H_6) = 6.8$ (6.8) eV, $T_d(CH_4) = 7.1$ (7.5) eV, and $T_d(H_2O) = 7.5$ (7.9) eV. The values for the constrained molecules proved to be slightly lower, as expected, because no energy can be transferred to the motion of the center of mass of the molecule. Then we used the McKinley–Feshbach formalism to calculate the cross-sections of radical formation (Methods) using the computed values of T_d as input parameters and compared them with the experimental data. For a range of organic hydrogen-containing molecules, the dependence of the simulated cross-section on electron energy (curves in Figure 3a) was found to be very similar to the experimentally observed energy dependence of the localized state density inferred from the E- to A-peak ratio (points in Figure 3a). We further investigated the energetics for adsorption of different single atoms (H, C, N, O, and Si) and radicals (OH, CH_2, CH_3, C_6H_5, and SiH) on the pristine MoS_2 monolayer. The DFT results indicate that adsorption of oxygen and carbon atoms are strongest among the considered ad-atoms (Figure S7, Supporting Information), corresponding to the binding energy of 3.96 and 2.64 eV, respectively. Also, the binding energy follows the order O > C > N > Si > H. In the case of radicals, the most favorable binding was found for CH_2 and SiH adsorption with an energy gain of 1.85 and 1.15 eV (Figure S8, Supporting Information). Our electronic structure calculations showed both carbon and silicon adatoms produce states at the conduction band minimum (0.18 and 0.24 eV respectively below the minimum) while oxygen has little influence on the density of states (Figure S7, Supporting Information). Qualitatively similar signatures are seen for radicals containing C, Si, and H, such as CH_2, CH_3, C_6H_5, and SiH (Figure S8, Supporting Information). The position of the states in the gap obtained from the calculations is consistent with the experimentally-observed energy separation of E and A peaks (Figures 2a and S1, Supporting Information) and the response of PL to electrical doping (Figure 2b). The presence of such organic molecules is furthermore

confirmed by high-resolution electron energy loss spectroscopy (EELS) across the patterned region of MoS_2 on a TEM grid (**Figure 4**). It shows a fivefold increase of the oxygen and carbon content and a tripled amount of silicon in e-beam treated areas (Figure S9 and S10, Supporting Information). Maps of the Mo and S signals (Figure 4) do not show any variation between patterned and non-patterned regions beyond additional scattering on Si (Figure S10a), confirming the absence of e-beam induced structural defects. Again, these signatures point toward organic molecules interacting with the sample.

Overall, all our data suggest that the E peak is related to carbon- and silicon- containing radicals formed after ballistic displacement of hydrogen in residues on the sample surface. One possible scenario is that the E peak is a charge-transfer exciton between the TMD and the state provided by the organic radicals (Figure S7,S8, Supporting Information). In fact, such excitons with a binding energy similar to that of native excitons previously been observed between TMDs and organic molecules on their surfaces.[53,54] These excitons are expected to have properties similar to that of the E peak: they only appear in the presence of and change with the concentration of external materials (Figure S4, Supporting Information),[55,56] blueshift at high excitation powers (Figures 2a and S2b, Supporting Information),[57] and become a ground state at low temperature (Figures 2a and S1, Supporting Information). The state is expected to appear in a comparable spectral range in all TMD materials.

3. Conclusion

To conclude, we patterned bright, room-temperature, localized excitons in 2D semiconductors using conventional electron beam lithography. This easy-to-use method features nanoscale resolution along with the potential of wide tunability and scalability. We investigated the nature of the localized state using a combination of techniques and concluded that it is not related to structural defects in the TMD. Instead, the state emerges due to the ballistic displacement of hydrogen atoms from molecules present on the surface of the sample. The resulting organic radicals bonding to the

**ADVANCED
SCIENCE NEWS**
www.advancedsciencenews.com

**ADVANCED
FUNCTIONAL
MATERIALS**
www.afm-journal.de

TMD give rise to an in gap state. The E-peak-related state could be a charge transfer exciton formed between a hole in the TMD and an electron in such a state provided by the organic radical. The observation of this state opens many interesting possibilities. First, its expected out-of-plane orientation should result in a large Stark shift in an out-of-plane electric field, further extending its spectral tunability. In the future, it will be interesting to measure this shift to establish the dipole moment of the state. Second, the localized nature of the state and the narrowing of PL peaks hints at its use as a single quantum emitter in applications toward quantum technologies. Unlike previously-demonstrated TMD-based single-quantum emitters, the E state survives up to room temperature, potentially extending the applicability of the devices based on it. In addition, we expect the spectral position of the state to depend on electric field, which can be controlled in a transistor-type device. These traits may prove critical in realizing entangled-photon devices. Third, it will be interesting to controllably pattern closely spaced deterministic arrays of electrically controlled localized excitons and study the effects caused by exciton interactions. Finally, as the observed state originates from molecules localized right at the TMD's surface, we expect a stronger response to the dielectric screening compared to that of free excitons. Such a response, combined with the observed room-temperature photoluminescence and environmental stability, may be interesting for biological and chemical sensing.

4. Experimental Section

Fabrication: The MoS_2 on SiO_2 samples was obtained by mechanical exfoliation of bulk material (>99.9% pure synthetic crystals from HQ graphene) onto the 300 nm SiO_2/Si using scotch tape or PDMS methods. The samples were washed with acetone and IPA to remove the organic residues. Then, they were loaded into a Raith Pioneer II SEM/EBL for patterning. The dose and accelerating voltage specified in the main text with a beam current of 0.22 nA and 30 μm apertures were used. Patterning was done in the dot-by-dot regime with an 18.9 nm step between dots in a row and an 80 nm step between rows. Afterward, the presence of the E peak in the room temperature PL spectrum of the sample confirms successful modification. Finally, the samples were annealed in vacuum at 230 °C for ≈12 h.

Photoluminescence Spectroscopy: The room-temperature PL data (Figure 1 and 3) were measured with a XploRA™ HORIBA using 532 nm excitation at 16 μW focused into a diffraction limited spot (≈1 μm diameter). Low-temperature experiments were performed with the Witec Alpha confocal spectroscopy setup in an optical cryostat with 532 nm green laser excitation focused in a ≈0.6 μm diameter spot. Low power PL spectra were fitted with four exponentially modified Gaussians to account for phononic sidebands.

AFM: Mechanical cleaning (nanosqueegee) and topography scans were performed with a NanoWizard® AFM in ambient conditions. For nanosqueegee non-contact tips (Tap300Al-G from BudgetSensors) were used in the contact regime applying above 100 nN and contact tips (CONTPt-10 from NanoWorld) below 100 nN. The topography scan (Figure 1a) was taken in contact mode with a 2 nN setpoint, two consecutive scans were always recorded. Afterward, polynomial background subtraction and line matching were applied to the scan.

Theoretical Results: DFT calculations were performed using the Vienna ab-initio Simulation Package (VASP)[58,59] using the Perdew–Burke–Ernzerhof (PBE) exchange-correlation functional.[60] Ab-initio molecular dynamics simulations of the radical formation from small organic molecules were carried out with high accuracy (high precision, plane wave cutoff 400 eV, gamma point approximation for non-periodic system, time step 0.1 fs). For the calculation of the displacement cross-section from the displacement thresholds the McKinley-Feshbach formalism to account for thermal vibrations as discussed previously was employed.[61] Further details of the calculations can be found in Note S2 (Supporting Information).

STEM and EELS: The $2L$-MoS_2 sample was mechanically exfoliated on PDMS and transferred onto a Quantifoil grid. Prior to its insertion into the electron microscope, the sample was baked for several hours at an elevated temperature (≈130 °C) in a high vacuum (≈2×10^{-6} Torr). STEM-EELS experiments were carried out using a Nion HERMES microscope. This instrument was equipped with an aberration corrector, a cold-field-emission-gun, a monochromator at ground potential, and a hybrid-pixel direct-detection camera (Dectris ELA). For the spectra presented in the main text, an energy dispersion of 0.8 eV channel^{-1} was used and the acceleration voltage was 60 keV. The probe convergence and EEL spectrometer aperture semi-angles were both ≈36 mrad. To avoid influence from the amorphous carbon film of the TEM grid the spectra was acquired on suspended regions of the TMD, several tens of nanometers away from the film. Model-based quantification of the spectra was performed after multiple scattering deconvolution, using multi-linear least square fitting. The fitted model contains a power-law background function and Hartree-Slater generalized oscillator strength functions for the edges; carbon and oxygen K, silicon and sulfur L3-1, and molybdenum M5-1. In this manner, absolute values for atomic ratios were obtained for the above-mentioned species.[62,63]

Supporting Information

Supporting Information is available from the Wiley Online Library or from the author.

Acknowledgements

Conflict of Interest

The authors declare no conflict of interest.

Author Contribution

D.Y., K.G., and K.I.B. conceived and designed the experiments, D.Y., K.G. prepared the samples, A.E. and C.T.K. performed EELS, STEM measurements along with related modeling and analysis, D.Y., N.S., and J.P.R. performed AFM measurements and AFM mechanical cleaning, D.Y., K.G. and S.K. performed the optical measurements, D.Y. analyzed the optical and AFM data, M.J., S.K., M.G., and A.K. performed the calculations and help to rationalize the experimental data, D.Y. and K.I.B. wrote the manuscript with input from all coauthors.

**ADVANCED
SCIENCE NEWS**

www.advancedsciencenews.com

**ADVANCED
FUNCTIONAL
MATERIALS**

www.afm-journal.de

Data Availability Statement

The data that support the findings of this study are available from the corresponding author upon reasonable request.

Keywords

charge transfer excitons, defects, electron beam lithography, single photon emitters, TMDs

[1] T. Mueller, E. Malic, *npj 2D Mater. Appl.* **2018**, *2*, 29.

[2] G. Wang, A. Chernikov, M. M. Glazov, T. F. Heinz, X. Marie, T. Amand, B. Urbaszek, *Rev. Mod. Phys.* **2018**, *90*, 021001.

[3] X. Xu, W. Yao, D. Xiao, T. F. Heinz, *Nat. Phys.* **2014**, *10*, 343.

[4] P. Rivera, M. He, B. Kim, S. Liu, C. Rubio-Verdú, H. Moon, L. Mennel, D. A. Rhodes, H. Yu, T. Taniguchi, K. Watanabe, J. Yan, D. G. Mandrus, H. Dery, A. Pasupathy, D. Englund, J. Hone, W. Yao, X. Xu, *Nat. Commun.* **2021**, *12*, 871.

[5] Y. J. Zheng, Y. Chen, Y. L. Huang, P. K. Gogoi, M.-Y. Li, L.-J. Li, P. E. Trevisanutto, Q. Wang, S. J. Pennycook, A. T. S. Wee, S. Y. Quek, *ACS Nano* **2019**, *13*, 6050.

[6] Z. Li, X. Lu, D. F. Cordovilla Leon, Z. Lyu, H. Xie, J. Hou, Y. Lu, X. Guo, A. Kaczmarek, T. Taniguchi, K. Watanabe, L. Zhao, L. Yang, P. B. Deotare, *ACS Nano* **2021**, *15*, 1539.

[7] C. Chakraborty, N. Vamivakas, D. Englund, *Nanophotonics* **2019**, *8*, 2017.

[8] A. Srivastava, M. Sidler, A. V. Allain, D. S. Lembke, A. Kis, A. Imamoğlu, *Nat. Nanotechnol.* **2015**, *10*, 491.

[9] G. Moody, K. Tran, X. Lu, T. Autry, J. M. Fraser, R. P. Mirin, L. Yang, X. Li, K. L. Silverman, *Phys. Rev. Lett.* **2018**, *121*, 057403.

[10] A. Kumar, D. Yagodkin, N. Stetzuhn, S. Kovalchuk, A. Melnikov, P. Elliott, S. Sharma, C. Gahl, K. I. Bolotin, *Nano Lett.* **2022**, *21*, 712.

[11] Y.-M. He, O. Iff, N. Lundt, V. Baumann, M. Davanco, K. Srinivasan, S. Höfling, C. Schneider, *Nat. Commun.* **2016**, *7*, 13409.

[12] C. K. Dass, M. A. Khan, G. Clark, J. A. Simon, R. Gibson, S. Mou, X. Xu, M. N. Leuenberger, J. R. Hendrickson, *Adv. Quantum Technol.* **2019**, *2*, 1900022 .

[13] X. Liu, M. C. Hersam, *Nat. Rev. Mater.* **2019**, *4*, 669.

[14] L. A. Jauregui, A. Y. Joe, K. Pistunova, D. S. Wild, A. A. High, Y. Zhou, G. Scuri, K. De Greve, A. Sushko, C.-H. Yu, T. Taniguchi, K. Watanabe, D. J. Needleman, M. D. Lukin, H. Park, P. Kim, *Science* **2019**, *366*, 870.

[15] A. Hötger, J. Klein, K. Barthelmi, L. Sigl, F. Sigger, W. Männer, S. Gyger, M. Florian, M. Lorke, F. Jahnke, T. Taniguchi, K. Watanabe, K. D. Jöns, U. Wurstbauer, C. Kastl, K. Müller, J. J. Finley, A. W. Holleitner, *Nano Lett.* **2021**, *21*, 1040.

[16] X. Yu, H. Cheng, M. Zhang, Y. Zhao, L. Qu, G. Shi, *Nat. Rev. Mater.* **2017**, *2*, 17046.

[17] A. Raja, L. Waldecker, J. Zipfel, Y. Cho, S. Brem, J. D. Ziegler, M. Kulig, T. Taniguchi, K. Watanabe, E. Malic, T. F. Heinz, T. C. Berkelbach, A. Chernikov, *Nat. Nanotechnol.* **2019**, *14*, 832.

[18] K. Greben, S. Arora, M. G. Harats, K. I. Bolotin, *Nano Lett.* **2020**, *20*, 2544.

[19] J. Klein, J. Klein, A. Kuc, A. Nolinder, M. Altzschner, J. Wierzbowski, F. Sigger, F. Kreupl, J. J. Finley, U. Wurstbauer, A. W. Holleitner, M. Kaniber, *2D Mater.* **2018**, *5*, 011007.

[20] J. Klein, M. Lorke, M. Florian, F. Sigger, L. Sigl, S. Rey, J. Wierzbowski, J. Cerne, K. Müller, E. Mitterreiter, P. Zimmermann, T. Taniguchi, K. Watanabe, U. Wurstbauer, M. Kaniber, M. Knap, R. Schmidt, J. J. Finley, A. W. Holleitner, *Nat. Commun.* **2019**, *10*, 2755.

[21] E. Mitterreiter, B. Schuler, K. A. Cochrane, U. Wurstbauer, A. Weber-Bargioni, C. Kastl, A. W. Holleitner, *Nano Lett.* **2020**, *20*, 4437.

[22] A. Branny, S. Kumar, R. Proux, B. D. Gerardot, *Nat. Commun.* **2017**, *8*, 15053.

[23] L. Linhart, M. Paur, V. Smejkal, J. Burgdörfer, T. Mueller, F. Libisch, *Phys. Rev. Lett.* **2019**, *123*, 146401.

[24] N. P. Wilson, W. Yao, J. Shan, X. Xu, *Nature* **2021**, *599*, 383.

[25] K. L. Seyler, P. Rivera, H. Yu, N. P. Wilson, E. L. Ray, D. G. Mandrus, J. Yan, W. Yao, X. Xu, *Nature* **2019**, *567*, 66.

[26] X. Wang, J. Zhu, K. L. Seyler, P. Rivera, H. Zheng, Y. Wang, M. He, T. Taniguchi, K. Watanabe, J. Yan, D. G. Mandrus, D. R. Gamelin, W. Yao, X. Xu, *Nat. Nanotechnol.* **2021**, *16*, 1208.

[27] F. Cadiz, C. Robert, G. Wang, W. Kong, X. Fan, M. Blei, D. Lagarde, M. Gay, M. Manca, T. Taniguchi, K. Watanabe, T. Amand, X. Marie, P. Renucci, S. Tongay, B. Urbaszek, *2D Mater.* **2016**, *3*, 045008.

[28] T. Korn, S. Heydrich, M. Hirmer, J. Schmutzler, C. Schüller, *Appl. Phys. Lett.* **2011**, *99*, 102109.

[29] J. C. Meyer, C. O. Girit, M. F. Crommie, A. Zettl, *Appl. Phys. Lett.* **2008**, *92*, 123110.

[30] X. Shen, H. Wang, T. Yu, *Nanoscale* **2013**, *5*, 3352.

[31] G. Love, V. D. Scott, N. M. T. Dennis, L. Laurenson, *Scanning* **1981**, *4*, 32.

[32] K. F. Mak, K. He, C. Lee, G. H. Lee, J. Hone, T. F. Heinz, J. Shan, *Nat. Mater.* **2013**, *12*, 207.

[33] S. Mouri, Y. Miyauchi, K. Matsuda, *Nano Lett.* **2013**, *13*, 5944.

[34] T. Schmidt, K. Lischka, W. Zulehner, *Phys. Rev. B* **1992**, *45*, 8989 .

[35] J. Klein, M. Lorke, M. Florian, F. Sigger, L. Sigl, S. Rey, J. Wierzbowski, J. Cerne, K. Müller, E. Mitterreiter, P. Zimmermann, T. Taniguchi, K. Watanabe, U. Wurstbauer, M. Kaniber, M. Knap, R. Schmidt, J. J. Finley, A. W. Holleitner, *Nat. Commun.* **2019**, *10*, 2755.

[36] A. R. Klots, B. Weintrub, D. Prasai, D. Kidd, K. Varga, K. A. Velizhanin, K. I. Bolotin, *Sci. Reports* **2018**, *8*, 768.

[37] C. Fournier, A. Plaud, S. Roux, A. Pierret, M. Rosticher, K. Watanabe, T. Taniguchi, S. Buil, X. Quélin, J. Barjon, J.-P. Hermier, A. Delteil, *Nat. Commun.* **2021**, *12*, 3779.

[38] T. T. Tran, K. Bray, M. J. Ford, M. Toth, I. Aharonovich, *Nat. Nanotechnol.* **2016**, *11*, 37.

[39] A. Ciarrocchi, D. Unuchek, A. Avsar, K. Watanabe, T. Taniguchi, A. Kis, *Nat. Photonics* **2019**, *13*, 131.

[40] H.-P. Komsa, J. Kotakoski, S. Kurasch, O. Lehtinen, U. Kaiser, A. V. Krasheninnikov, *Phys. Rev. Lett.* **2012**, *109*, 035503.

[41] H.-P. Komsa, S. Kurasch, O. Lehtinen, U. Kaiser, A. V. Krasheninnikov, *Phys. Rev. B* **2013**, *88*, 35301.

[42] S. Kretschmer, T. Lehnert, U. Kaiser, A. V. Krasheninnikov, *Nano Lett.* **2020**, *20*, 2865.

[43] H.-P. Komsa, J. Kotakoski, S. Kurasch, O. Lehtinen, U. Kaiser, A. V. Krasheninnikov, *Phys. Rev. Lett.* **2012**, *109*, 035503.

[44] R. E. Palmer, P. J. Rous, *Rev. Mod. Phys.* **1992**, *64*, 383.

[45] M. R. Rosenberger, H.-J. Chuang, K. M. Mccreary, A. T. Hanbicki, S. V. Sivaram, B. T. Jonker, *ACS Appl. Mater. Interfaces* **2018**, *10*, 10379.

[46] Y. Lin, X. Ling, L. Yu, S. Huang, A. L. Hsu, Y.-H. Lee, J. Kong, M. S. Dresselhaus, T. Palacios, *Nano Lett.* **2014**, *14*, 5569.

[47] A. Branny, S. Kumar, R. Proux, B. D. Gerardot, *Nat. Commun.* **2017**, *8*, 5569.

[48] T. P. Darlington, C. Carmesin, M. Florian, E. Yanev, O. Ajayi, J. Ardelean, D. A. Rhodes, A. Ghiotto, A. Krayev, K. Watanabe, T. Taniguchi, J. W. Kysar, A. N. Pasupathy, J. C. Hone, F. Jahnke, N. J. Borys, P. J. Schuck, *Nat. Nanotechnol.* **2020**, *15*, 854.

[49] M. Kremser, M. Brotons-Gisbert, J. Knörzer, J. Gückelhorn, M. Meyer, M. Barbone, A. V. Stier, B. D. Gerardot, K. Müller, J. J. Finley, *npj 2D Mater. Appl.* **2020**, *4*.

[50] A. V. Tyurnina, D. A. Bandurin, E. Khestanova, V. G. Kravets, M. Koperski, F. Guinea, A. N. Grigorenko, A. K. Geim, I. V. Grigorieva, *ACS Photonics* **2019**, *6*, 516.

[51] Y.-C. Lin, D. O. Dumcenco, Y.-S. Huang, K. Suenaga, *Nat. Nanotechnol.* **2014**, *9*, 391 .

[52] S. W. Han, Y. Park, Y. H. Hwang, S. Jekal, M. Kang, W. G. Lee, W. Yang, G.-D. Lee, S. C. Hong, *Sci. Rep.* **2016**, *6*, 38730.

[53] T. Zhu, L. Yuan, Y. Zhao, M. Zhou, Y. Wan, J. Mei, L. Huang, *Sci. Adv.* **2018**, *4*, 1.

[54] T. R. Kafle, B. Kattel, S. D. Lane, T. Wang, H. Zhao, W.-L. Chan, *ACS Nano* **2017**, *11*, 10184.

[55] M. Lunz, A. L. Bradley, W.-Y. Chen, V. A. Gerard, S. J. Byrne, Y. K. Gun'ko, V. Lesnyak, N. Gaponik, *Phys. Rev. B* **2010**, *81*.

[56] C. R. Kagan, C. B. Murray, M. G. Bawendi, *Phys. Rev. B* **1996**, *54*, 8633.

[57] P. Nagler, G. Plechinger, M. V. Ballottin, A. Mitioglu, S. Meier, N. Paradiso, C. Strunk, A. Chernikov, P. C. M. Christianen, C. Schüller, T. Korn, *2D Mater* **2017**, *4*, 025112.

[58] G. Kresse, D. Joubert, *Phys. Rev. B* **1999**, *59*, 1758.

[59] G. Kresse, J. Furthmüller, *Phys. Rev. B* **1996**, *54*, 11169.

[60] J. P. Perdew, K. Burke, M. Ernzerhof, *Phys. Rev. Lett.* **1996**, *77*, 3865.

[61] J. C. Meyer, F. Eder, S. Kurasch, V. Skalakova, J. Kotakoski, H. J. Park, S. Roth, A. Chuvilin, S. Eyhusen, G. Benner, A. V. Krasheninnikov, U. Kaiser, *Phys. Rev. Lett.* **2012**, *108*, 196102.

[62] R. F. Egerton, *Electron Energy-Loss Spectroscopy in the Electron Microscope. Electron Energy-Loss Spectroscopy in the Electron Microscope*, Springer, New York **2011**.

[63] F. D. L. Peña, E. Prestat, V. T. Fauske, P. Burdet, P. Jokubauskas, M. Nord, T. Ostasevicius, K. E. MacArthur, M. Sarahan, D. N. Johnstone, J. Taillon, J. Lähnemann, V. Migunov, A. Eljarrat, J. Caron, T. Aarholt, S. Mazzucco, M. Walls, T. Slater, F. Winkler, B. Pquinn-Dls, Martineau, G. Donval, R. McLeod, E. R. Hoglund, I. Alxneit, D. Lundeby, T. Henninen, L. F. Zagonel, A. Garmannslund, hyperspy/hyperspy: Release v1.6.1. **2020**, https://doi.org/10.5281/ZENODO.4294676.